Al-Nahrain Journal of Science
ANJS, Vol.28 (4), December, 2025, pp. 13-32

In Silico and In Vitro Studies Unveil the Protective Potential of Diosmin-Hesperidin Conjugate in Doxorubicin Toxicity

Adejuwon A. Adeneye[1,2,*], Taiwo M. Abdulrafiu[1]

[1] Department of Pharmacology, Therapeutics and Toxicology, Faculty of Basic Clinical Sciences, Lagos State University College of Medicine, Ikeja, Lagos State, Nigeria
[2] Directorate of Research Management and Innovation, Office of the Vice Chancellor, 3rd Floor, Babatunde Raji Fashola Senate Building, Main Campus, Lagos State University, Ojo, Lagos State, Nigeria

Article's Information

Received: 21.12.2024
Accepted: 19.11.2025
Published: 15.12.2025

Keywords:
Diosmin-Hesperidin Conjugate,
Doxorubicin Toxicity,
Oxidative Stress,
Antioxidant Activity,
In Silico and In Vitro Studies.

Abstract/ Overview

Doxorubicin (DOX), a potent anthracycline antibiotic widely used in cancer therapy, is notorious for inducing off-target multi-organ toxicities. These toxicities arise through mechanisms such as DNA intercalation, topoisomerase II poisoning, oxidative stress via free radical generation, and membrane disruption caused by altered sphingolipid metabolism. Mitigating these adverse effects is essential to improving the therapeutic index of DOX. This study investigates the protective potential of a diosmin-hesperidin conjugate using in silico and in vitro methods. The diosmin-hesperidin conjugate, derived from natural flavonoids, was assessed for its anti-apoptosis and antioxidant potential to alleviate DOX-induced toxicities. In silico analyses, including molecular docking and dynamic simulations, revealed high binding affinities of the conjugate to key oxidative stress-related targets, such as catalase, glutathione reductase, and apoptosis-related proteins (e.g., caspase-3, Hsp70, and Hsp90ß). In vitro assays, including DPPH, NO scavenging, FRAP, H_2O_2 scavenging, lipid peroxidation inhibition, and total antioxidant capacity, validated the conjugate's robust antioxidant activity. The computational and in vitro studies showed that the conjugate stabilized antioxidant enzymes and inhibited apoptotic pathways. Overall, by leveraging the synergistic effects of this flavonoid conjugate, this study highlighted the diosmin-hesperidin conjugate as a promising natural adjunct therapy to mitigate DOX's off-target oxidative stress- and apoptosis-mediated toxicities. Thus, providing a foundation for further preclinical and clinical evaluations, and contributing to the advancement of natural product-based cancer therapy.

http://doi.org/10.22401/ANJS.28.4.02
*Corresponding author: adejuwon.adeneye@lasucom.edu.ng

1. Introduction

Doxorubicin (DOX) (Figure 1), a powerhouse anthracycline antibiotic, remains a linchpin in the treatment of both solid and hematological malignancies, thanks to its formidable anti-cancer properties [1-3]. However, its clinical utility is significantly hampered by severe, dose-independent, multi-organ toxicities, most notably cardiotoxicity, hepatotoxicity, and nephrotoxicity, which collectively threaten patient outcomes [1,3-4]. DOX exerts its cytotoxic effects through multiple mechanisms, including DNA intercalation, topoisomerase II inhibition, mitochondrial dysfunction, and ROS generation, leading to oxidative stress and apoptotic cell death [3-4]. However, at the heart of these deleterious effects lies oxidative stress, fueled by excessive reactive oxygen species (ROS) generation, making the quest

for effective protective strategies an urgent priority in cancer treatment [5].

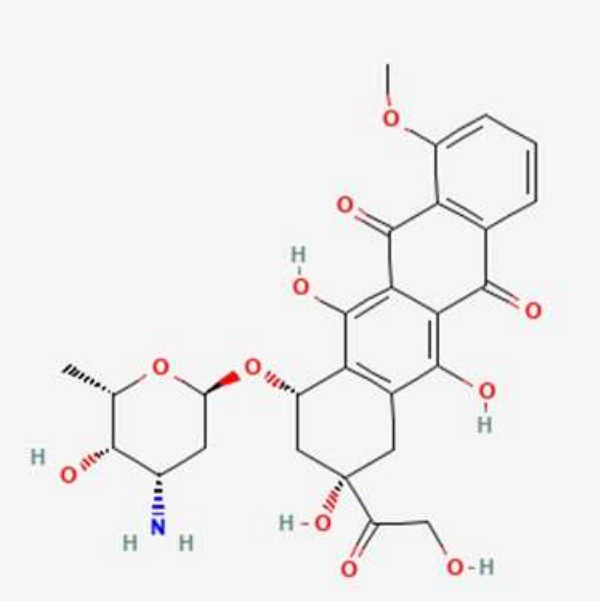

Figure 1. The two-dimension (2-D) chemical structure of doxorubicin (source: https://pubchem.ncbi.nlm.nih.gov/compound/Doxorubicin)

Natural antioxidants, particularly flavonoids, have emerged as compelling contenders in the fight against oxidative damage. Among them, diosmin and hesperidin, abundant in citrus fruits, possess potent antioxidant, anti-inflammatory, and cytoprotective properties [6]. While individually powerful, preclinical or pharmacokinetic studies have demonstrated an improved absorption, metabolism, or bioactivity of the diosmin-hesperidin conjugate over its individual components, thereby offering greater antioxidant and anti-inflammatory effects in oxidative stress-related disorders [7-9]. Daflon®, a micronized purified flavonoid fraction comprising 90% diosmin and 10% hesperidin, is commercially available across France, Spain, Malaysia, Belgium, as well as numerous African countries where it is widely utilized in the clinical management of vascular diseases such chronic venous insufficiency, venous ulcers, and hemorrhoids where it has shown impressive clinical efficacy. However, its role in mitigating chemotherapy-induced oxidative damage remains unexplored, necessitating further investigation. Also, several antioxidants, including curcumin, N-acetylcysteine, and quercetin, have been investigated for their protective roles against DOX-induced oxidative stress [10-11]. Diosmin and hesperidin, due to their unique pharmacokinetics and potent antioxidant properties, may offer comparable or superior cytoprotective effects, warranting further study (Morgan et al., 2023) [12]. A paradigm shift in drug discovery and toxicology has been catalyzed by the convergence of computational (*in silico*) and experimental (*in vitro*) methodologies. Molecular docking and dynamic simulations provide predictive insights into compound-target interactions, illuminating potential mechanisms of action [13-19]. Meanwhile, *in vitro* studies serve as a crucial validation tool, deciphering biochemical and cellular responses in real-world biological systems [20-22]. By harnessing both approaches, a holistic understanding of a compound's therapeutic profile can be achieved, bridging the gap between theoretical promise and clinical applicability. With the global burden of cancer escalating and chemotherapy-induced toxicities remaining a major clinical challenge, this study aligns with the overarching goal of optimizing therapeutic efficacy while mitigating adverse effects. This study aims to explore the antioxidant and protective potential of the diosmin-hesperidine conjugate against DOX-induced toxicities via molecular docking studies of the pathways involved in DOX cytotoxicity. Specifically, the exploratory study investigates the molecular interactions and binding affinities of the diosmin-hesperdine conjugate with key antioxidant and oxidative stress-related targets via *in silico* analysis; evaluates its ROS-scavenging capacity and ability to counteract oxidative damage *in vitro*; and assesses its protective effects in cellular models subjected to DOX-induced oxidative stress. Thus, this study explores the potential of the diosmin-hesperidin conjugate as a natural antioxidant therapy that may contribute to reducing DOX-induced toxicity, pending further preclinical and clinical evaluation.

2. Experimental

The workflow for investigating the molecular docking and *in vitro* antioxidant properties of a diosmin-hesperidin conjugate is schematically presented as Scheme 1. This representation provides a comprehensive overview of the sequential processes, from computational ligand-receptor interactions to experimental assays designed to elucidate the conjugate's pharmacological potential.

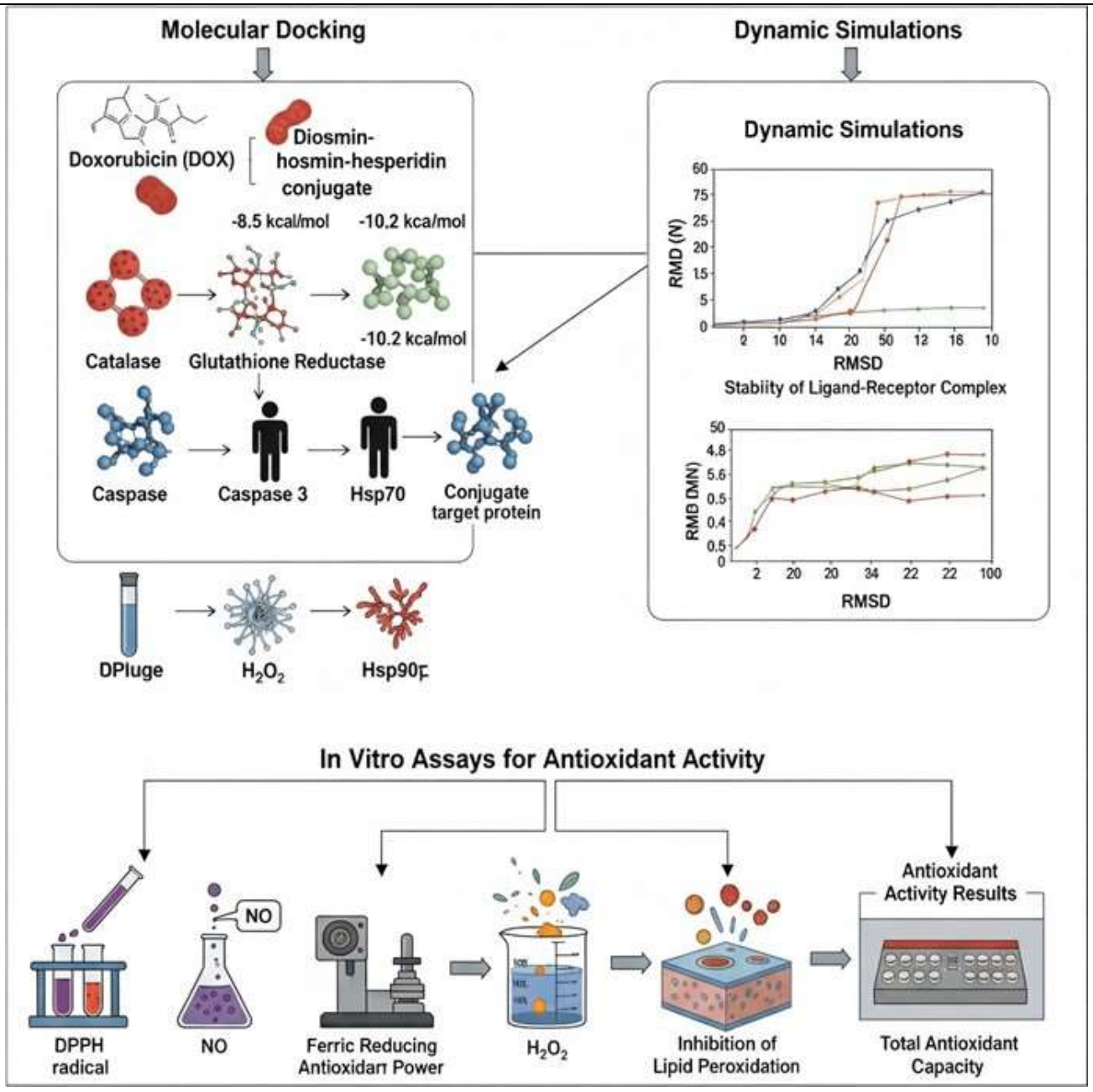

Scheme 1. The workflow for the molecular docking and *in vitro* antioxidant properties of a diosmin-hesperidin conjugate in doxorubicin toxicity.

2.1. Blind Molecular Docking Protocol for the Diosmin-Hesperidin Conjugate (Daflon®)

2.1.1. Retrieval and preparation of target protein 3d structures

The three-dimensional (3D) crystallographic structures of the selected protein targets (as specified in Table 1) were sourced from the Research Collaboratory for Structural Bioinformatics Protein Data Bank (RCSB-PDB) (https://www.rcsb.org/). Post-retrieval, structural refinement was carried out using PyMol toolkits, ensuring optimized visualization. The precise binding pocket coordinates for each protein were delineated using the PyRx AutoDock Vina software (version: 1.2.0), allowing for accurate molecular docking grid definition [16].

2.1.2. Acquisition and preparation of ligands

The molecular structure files for diosmin (PubChem CID: 5281613), hesperidin (PubChem ID: 10621), and their corresponding reference inhibitors or activators, as detailed in Table 1, were retrieved from the NCBI PubChem database (https://pubchem.ncbi.nlm.nih.gov/). The diosmin-hesperidin complex was synthesized computationally through molecular conjugation using the Schrödinger merger tool (which is part of the broader Schrödinger software suite). Following this, ligand structures were converted from MOL SDF format to PDBQT files via Open Babel, an integrated function within PyRx. This conversion enabled the generation of atomic coordinate descriptors. Ligand structures were subjected to energy minimization using the PyRx platform's Open Babel toolkit, which employed the Universal Force Field (UFF). A total of 2500 steps were set for the minimization, with Kohlmann and Gasteiger partial charges assigned to optimize molecular conformation and stability [16].

2.1.3. Blind molecular docking strategy for the diosmin-hesperidin conjugate

Molecular docking simulations were conducted using PyRx AutoDock Vina, employing an exhaustive search algorithm to anchor the ligand-receptor interactions. The grid box center was set at least 20A˚ so as to ensure it covers all key residues of the binding pocket. The exhaustiveness value was increased from the default of 8 to 16 so as to give more accurate and reliable results. The docking process was guided by empirical scoring functions influenced by the Nelder-Mead Simplex optimization algorithm, systematically applied across varying grid resolutions following the reduction model proposed by Trott and Olson [16]. Blind docking was employed to conduct an unbiased, exploratory evaluation of a novel conjugate's binding propensities across a panel of diverse protein targets, including caspase-3, catalase, Hsp 70, Hsp 90ß, and VCAM-1. This system-agnostic approach enabled a comprehensive scan of entire protein surfaces to identify potential interactions at both orthosteric and allosteric sites, mitigating bias from preconceived binding location hypotheses. The strategy facilitated a comparative analysis of the conjugate's thermodynamically favorable binding poses across multiple targets, providing insight into its potential polypharmacological mechanisms of action.

2.1.4. Protein-ligand binding affinity assessment and interaction visualization

To validate the docking protocol, established reference ligands were first docked into their cognate active sites. Their binding modes were then comparatively analyzed against the test compounds using identical grid parameters to ensure methodological consistency. The resulting poses were visualized via scatter plots (Osiris Data Warrior) and their three-dimensional interaction profiles were elucidated using PyMOL. For a granular analysis, two-dimensional interaction diagrams, including hydrophobic contacts, were generated with BIOVIA Discovery Studio. The most thermodynamically stable conformation for each ligand, corresponding to the lowest binding energy pose, was selected for detailed analysis of the key molecular interactions.

Table 1: Study Targets and their Corresponding Standard Modulators

Target Protein	Protein Data Bank (PDB) Identifier	Gene Source	Standard Ligand/Compound
BCL-2-associated X Protein (BAX)	MSN-125	Homo sapiens	MSN-125/I*
Caspase-3	3KJF	Homo sapiens	VRT-043198/I*
Catalase	Human erythrocyte catalase 3-amino-1,2,4-triazole complex (1DGH)	Homo sapiens	Metformin/A*
Glutathione Reductase	1GRE	Homo sapiens	Oxiglutathione/A*
Vascular Cell Adhesion Molecule 1 (VCAM 1)	1VSC	Homo sapiens	BDBM50105195/I*
I* - Inhibitor; A* - Activator			

2.2. In vitro antioxidant assays

2.2.1 Antioxidant scavenging assay

The antioxidant potential of the diosmin-hesperidin conjugate was assessed through multiple standardized methods, including the DPPH, nitric oxide (NO) scavenging, ferric reducing antioxidant power (FRAP), and total antioxidant capacity (TAC) assays.

2.2.1.1. DPPH Radical Scavenging Assay

The free radical scavenging capacity of the diosmin-hesperidin conjugate was quantitatively assessed using the 1,1-diphenyl-2-picryl-hydrazyl (DPPH) assay. The assay measures the ability of a compound to donate a hydrogen atom, thereby reducing the stable DPPH radical, which results in a spectrophotometrically measurable decrease in absorbance. A 0.1 mM (100 µM) methanolic DPPH solution was employed, with ascorbic acid serving as the reference standard. The percentage inhibition of DPPH radical formation was determined for test concentrations ranging from 25 to 100 µg/mL. The concentration required to achieve 50% radical scavenging activity (IC_{50} value) was then calculated by interpolating from a dose-response curve generated by plotting the percentage inhibition against the corresponding sample concentration [20].

The formula for the calculation the DPPH %inhibition is as follows:

$$DPPH\%\ Inhibition = \frac{A_{Control} - A_{Sample\ A\ Control}}{A_{Control}} \times 100$$

where $A_{control}$ represents the absorbance of the DPPH solution in distilled water of 517 nm, and A_{sample} corresponds to the absorbance of the diosmin-hesperidin-DPPH reaction mixture.

2.2.1.2. Nitric Oxide (NO) Scavenging Assay

This test assessed the conjugate's capacity to scavenge nitric oxide radicals, which were generated from sodium nitroprusside. The Griess reaction assay was used to quantify the remaining NO levels [21].

2.2.1.3. Ferric Reducing Antioxidant Power (FRAP) Assay

This assay determined the conjugate's reducing power by measuring its ability to reduce ferric (Fe^{3+}) ions to their ferrous (Fe^{2+}) form, following a modified protocol by Oyaizu [22].

2.2.1.4. Quantification of Nitric Oxide (NO) Levels

To indirectly measure and quantify nitric oxide levels in diosmin-hesperidin aliquots, the Griess reaction assay was employed, following the method established by Vishwakarma *et al.* [23].

2.2.1.5. Lipid Peroxidation Inhibition via TBARS Assay

The conjugate's ability to inhibit lipid peroxidation was evaluated using the TBARS assay, which measures the formation of malondialdehyde (MDA), a product of lipid peroxidation as described by Hussen and Endalew [20]. The inhibition percentage was calculated using the following formula:

$$\%\ Lipid\ Peroxidation\ Inhibition = 100 - A_{Sample} \times 100$$

2.2.1.6. Hydrogen Peroxide (H_2O_2) Scavenging Assay

This assay quantified the conjugate's ability to neutralize hydrogen peroxide by measuring the reduction in its concentration after reacting with the conjugate at various concentrations (25-100 µg/mL) to determine the IC_{50} value [20].

$$H_2O_2\%\ Scavenging = \frac{A_{Blank} - A_{Sample}}{A_{Blank}} \times 100$$

A_{blank} is the absorbance of the blank and A_{sample} is absorbance of either the standard drug or diosmin-hesperidin conjugate. All experiments were conducted in quadruplicate to ensure statistical reliability. The results from these assays collectively provide a comprehensive profile of the diosmin-hesperidin conjugate's antioxidant properties.

2.3. Data Analysis

Statistical analysis was performed using GraphPad Instat software (version 5.0, GraphPad Prism Inc., San Diego, CA, U.S.A.). Results were expressed as mean ± standard error of the mean (SEM). One-way ANOVA was employed to evaluate statistical significance across treatment groups, followed by Tukey's post-hoc test for pairwise comparisons. For molecular docking analysis, hydrophobic interactions between ligand atoms and target protein residues, along with two-dimensional interaction mapping, were analyzed using BIOVIA Discovery Studio (version 17.2.0.16349, Dassault Systèmes, Vélizy-Villacoublay, France), as per the method described by Du *et al.* [18]. The docking protocol was first rigorously validated through redocking of a native crystallographic ligand, achieving a root-mean-square deviation (RMSD) of ≤2.0 Å, which confirmed the accuracy of the parameters for pose prediction. Subsequently, the most energetically favorable binding conformation

for the diosmin-hesperidin conjugate was identified based on the local minimum energy state and further validated for stability through molecular dynamics simulations [24].

3. Results

3.1. *In silico* studies of the binding energy and binding pathways of diosmin, hesperidin, and diosmin-hesperidin conjugate

3.1.1 Binding energy result of diosmin, hesperidin, diosmin-hesperidin conjugate, and VRT-043198 on caspase 3 following docking simulations. The binding affinities of the docked drugs were relatively higher than those of VRT-043198 (the standard) (-6 Kcal/mol) on caspase-3 protein, with diosmin-hesperidin complex exhibiting the highest binding affinity (Figure 2A). Diosmin binds to Arg 164, Lys 156, and Asp 135 of caspase 3 protein with conventional hydrogen bond at the bond distances of 3.24 Å, 2.77 Å, and 2.38 Å, respectively, in addition to Lys 137 and Phe 158 at the bond distances of 4.18 Å and 4.96 Å, respectively, following docking of the compounds into caspase-3 protein (Figures 3Ai-3Aii). Hesperidin binds to Lys 156, Thr 140, and Phe 158 of caspase-3 protein with conventional hydrogen bond at the average bond distances of 2.04 Å, 2.02 Å, and 3.42 Å respectively; Ile 159 and Ile 160 through the Pi-Alkyl bond at the bond distances of 4.44 Å and 5.10 Å respectively, as well as Arg 164 through the relatively more hydrophobic Pi-Cation bond at the bond distance of 3.64 Å, following docking of the compounds into caspase 3 protein (Figures 3Bi-3Bii). Diosmin-hesperidin conjugate binds to Phe 158 and Thr 140 of caspase 3 protein with conventional hydrogen bond at the average bond distances of 2.17 Å and 2.12 Å respectively; Leu 136 and Lys 156 through the Pi-Alkyl bond at the bond distances of 5.38 Å and 5.25 Å respectively; Arg 164 and Glu 124 through the relatively more hydrophobic Pi-Anion bond at the respective bond distances of 4.20 Å and 3.70 Å, as well as Ile 160 through the Pi-Donor hydrogen bond at the average bond distance of 3.44 Å following docking of the drugs into caspase 3 protein (Figures 3Ci-3Cii). VRT-043198 binds to Asp 135, Ala 162, Gly 125, and Ile 160 of caspase 3 protein with conventional hydrogen bond at the average bond distances of 2.13 Å, 3.13 Å, 2.57 Å, and 2.87 Å respectively; Leu 136 through the relatively more hydrophobic Pi-Alkyl bond at the bond distance of 4.66 Å, as well as Arg 164 through the hydrophobic Pi-Cation bond at the bond distance of 4.21 Å, following docking of the compounds into caspase 3 protein (Figures 3Di-3Dii).

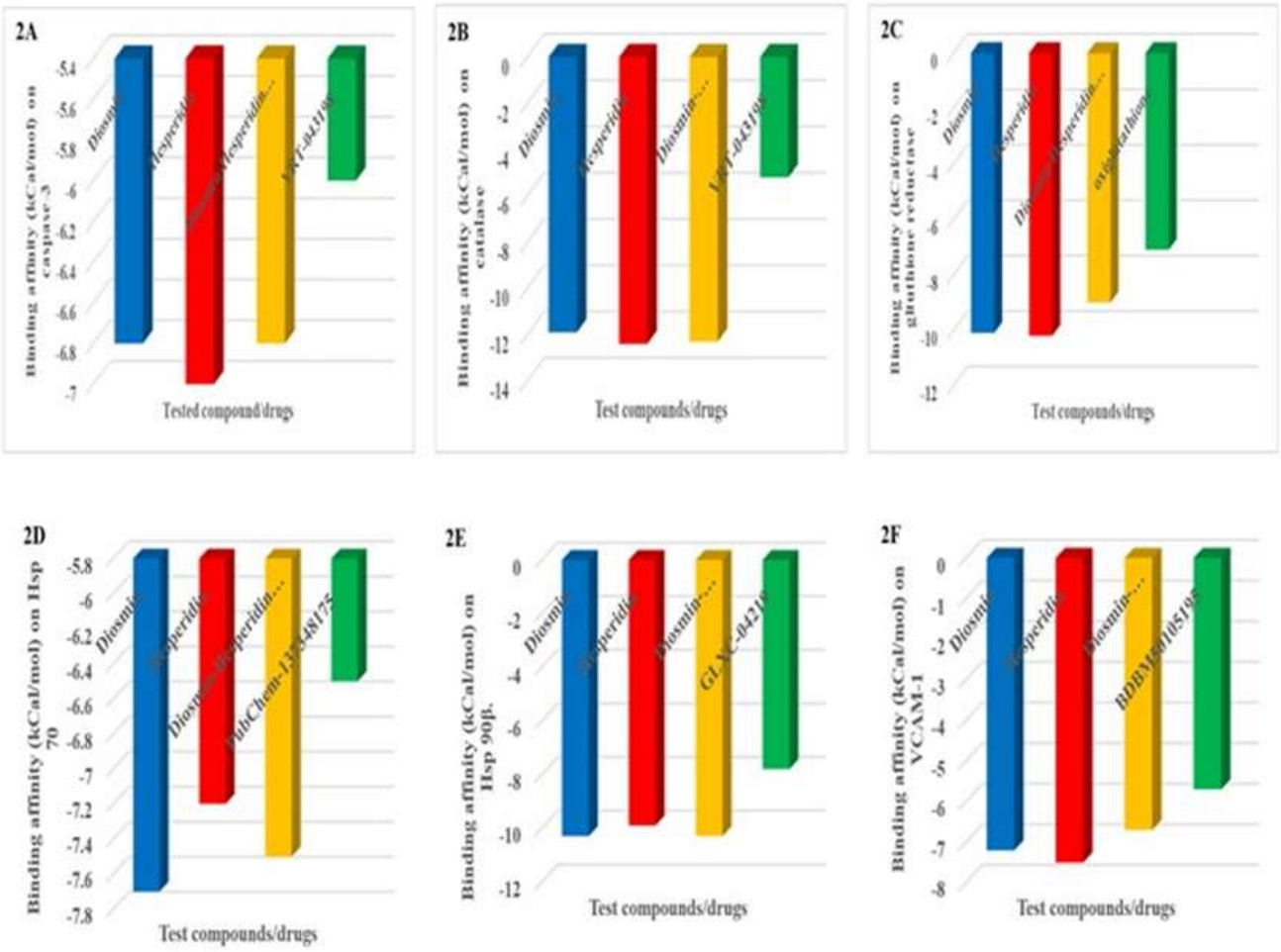

Figure 2. Molecular docking analysis of diosmin, hesperidin, and their conjugate against key doxorubicin toxicity-associated proteins. The panels present the calculated binding affinities (kcal/mol) of diosmin, hesperidin, and the diosmin-hesperidin conjugate to a panel of proteins implicated in doxorubicin-induced toxicities. (2A): Binding affinities for caspase-3, a key effector of apoptosis. The standard drug is VRT-043198; (2B): Binding affinities for catalase, an antioxidant enzyme that converts hydrogen peroxide to water and oxygen. The standard drug is VRT-043198; (2C): Binding affinities for glutathione reductase, a crucial enzyme in the cellular antioxidant defense system. The standard drug is oxiglutathione; (2D): Binding affinities for Hsp70 and Hsp90ß, two molecular chaperones that regulate protein stability. The standard inhibitors are PubChem-137348175 and GLXC-04219, respectively. (2E): Binding affinities for VCAM-1 (Vascular Cell Adhesion Molecule 1), an adhesion molecule implicated in inflammation. The standard drug is BDBM50105195.

The binding affinities were determined through molecular docking simulations, with more negative values indicating a stronger binding interaction.

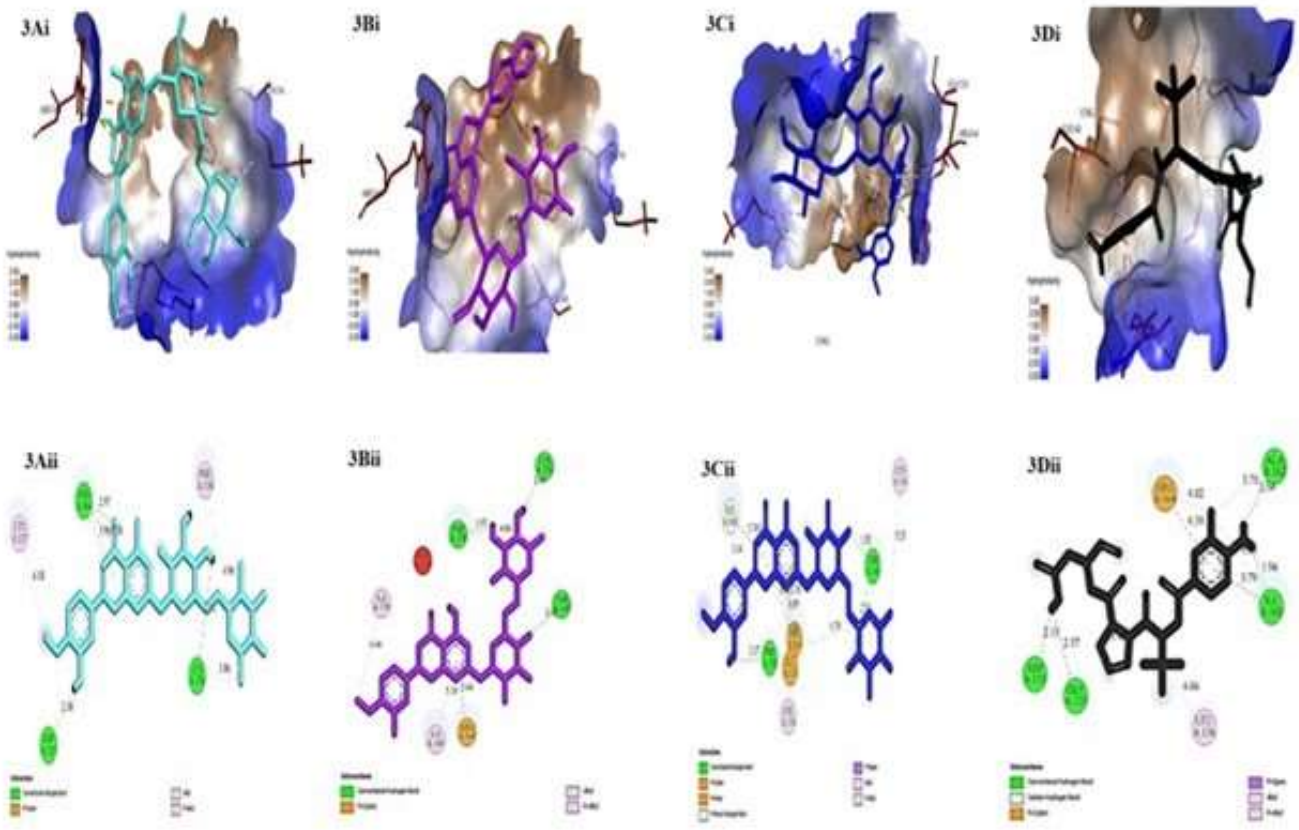

Figure 3. Binding modes and key interactions of diosmin, hesperidin, and their conjugate with caspase-3. The figure illustrates the molecular interactions between diosmin, hesperidin, their conjugate, and the standard inhibitor VRT-043198 within the active site of caspase-3, as determined by molecular docking simulations. **(3A).** Diosmin shows its interaction with the binding pocket of caspase-3; **(3Ai)** A pocket hydrophobicity view highlights the hydrophobic and hydrophilic regions of the binding site; **(3Aii)** A 2-D diagram shows the specific hydrogen bonds and hydrophobic interactions between diosmin and key amino acid residues of caspase-3. **(3B).** Hesperidin shows its interaction with the binding pocket of caspase-3: **(3Bi)** The hydrophobicity map of the binding pocket is shown; **(3Bii)** A 2D diagram depicts the specific interactions between hesperidin and the caspase-3 enzyme. **(3C).** The diosmin-hesperidin conjugate shows its interaction with the binding pocket of caspase-3; **(3Ci)** The hydrophobicity map of the binding pocket is shown; **(3Cii)** A 2D diagram depicts the specific interactions between the conjugate and the caspase-3 enzyme. **(3D).** The standard inhibitor VRT-043198 shows its interaction with the binding pocket of caspase-3; **(3Di)** The hydrophobicity map of the binding pocket is shown; **(3Dii)** A 2D diagram depicts the specific interactions between the inhibitor and the caspase-3 enzyme.

This figure provides a detailed, atomic-level view of how each compound fits into and interacts with the caspase-3 active site, helping to explain their potential biological activity.

3.1.2. Binding energy result of diosmin, hesperidin, diosmin-hesperidin conjugate, and VRT-043198 on catalase following docking simulations. The binding affinities of the docked compounds were relatively higher than those of metformin (the standard catalase activator) (-5.2 Kcal/mol) on catalase protein, with hesperidin exhibiting the highest binding affinity (Figure 2B). Hesperidin binds to Tyr 358, Arg 354, Arg 112, Ser 114, His 75, Arg 65 of catalase protein with conventional hydrogen bond at the average bond distances of 4.68 Å, 4.72 Å, 2.39 Å, 3.25 Å, and 2.31 Å respectively. This is in addition to binding to Ala 357, Val 74, and Val 146 of the protein through the hydrophobic alkyl bond at the average distances of 4.58 Å, 5.37 Å, and 4.86 Å, as well as Phe 153 and Phe 161 through the Pi-Pi stacked bond at the bond distance of 4.37 Å

and 5.03 Å, following docking of the compounds into the catalase protein (Figures 4Ai-4Aii). Metformin binds to Tyr 358 and Gly 147 of catalase protein with conventional hydrogen bond at the average bond distances of 3.01 Å and 2.73 Å. This is in addition to binding to His 75 of the protein through the hydrophobic Pi-cation bond at the bond distance of 3.58 Å, following docking of the compounds into the catalase protein (Figures 4Bi-4Bii).

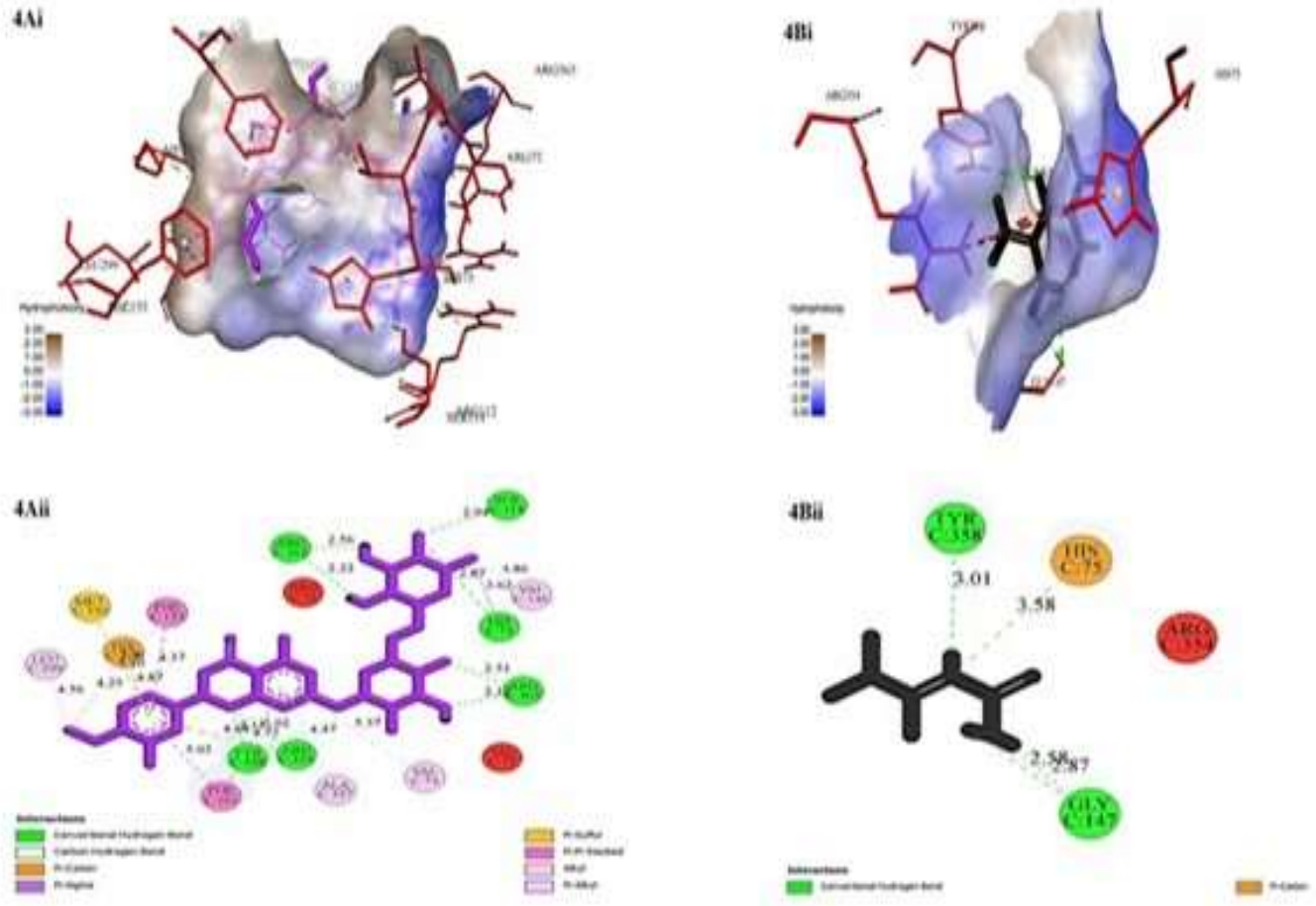

Figure 4. Molecular docking analysis of hesperidin and metformin binding to catalase. This figure illustrates the distinct binding interactions of hesperidin and metformin with the catalytic pocket of the antioxidant enzyme, catalase. **4A.** Hesperidin-catalase interaction; **(4Ai)** A hydrophobicity map of the catalase binding pocket, highlighting the hydrophobic and hydrophilic regions that accommodate hesperidin; **(4Aii)** A 2D schematic of the molecular interactions, showing the specific amino acid residues of catalase involved in binding to hesperidin and the types of bonds formed (e.g., hydrogen bonds).
4B. Metformin-catalase Interaction. **(4Bi)** A hydrophobicity map of the catalase binding pocket, revealing how the pocket accommodates the binding of metformin; **(4Bii)** A 2D schematic detailing the specific molecular interactions between metformin and the amino acid residues within the catalase binding pocket.

These representations provide key insights into the pharmacological binding mechanism and potential inhibitory effects of each compound on catalase function.

3.1.3. Binding energy results of diosmin, hesperidin, diosmin-hesperidin conjugate, and oxiglutathione on glutathione reductase following docking simulations. The binding affinities of the docked compounds were relatively higher than those of oxiglutathione (the standard) (-7.1 Kcal/mol) on glutathione reductase protein, with hesperidine exhibiting the highest binding affinity (Figure 2C). Hesperidin binds to Leu 338, Asp 331, Cys 58, Cys 63, Thr 339, Lys 66, and Lys 67 of glutathione reductase protein with conventional hydrogen bond

at the average bond distances of 3.71 Å, 2.21 Å, 3.81 Å, and 3.40 Å, 2.77 Å, 2.27 Å, 3.87 Å respectively; Val 64 and Pro 340 through the relatively more hydrophobic Pi-Alkyl bond at the bond distances of 3.87 Å and 5.47 Å, as well as Gly 62 through the carbon-hydrogen bond at the bond distance of 3.34 Å, following docking of the compounds into glutathione reductase protein (Figures 5Ai-5Aii). Oxiglutathione binds to Ser 177, Thr 57, Cys 58, Ser 30, Lys 66, Pro 368, and Tyr 197 of glutathione reductase protein through the conventional hydrogen bond at the average bond distances of 2.68 Å, 1.94 Å, 1.95 Å, 2.40 Å, 2.17 Å, 2.42 Å, and 2.50 Å respectively; Leu 338 through the relatively more Alkyl bond at the bond distance of 5.12 Å, as well as Cys 63 of the protein through the carbon-hydrogen bond at the bond distance of 4.28 Å, following docking of the compounds into glutathione reductase protein (Figure 5Bi-5Bii).

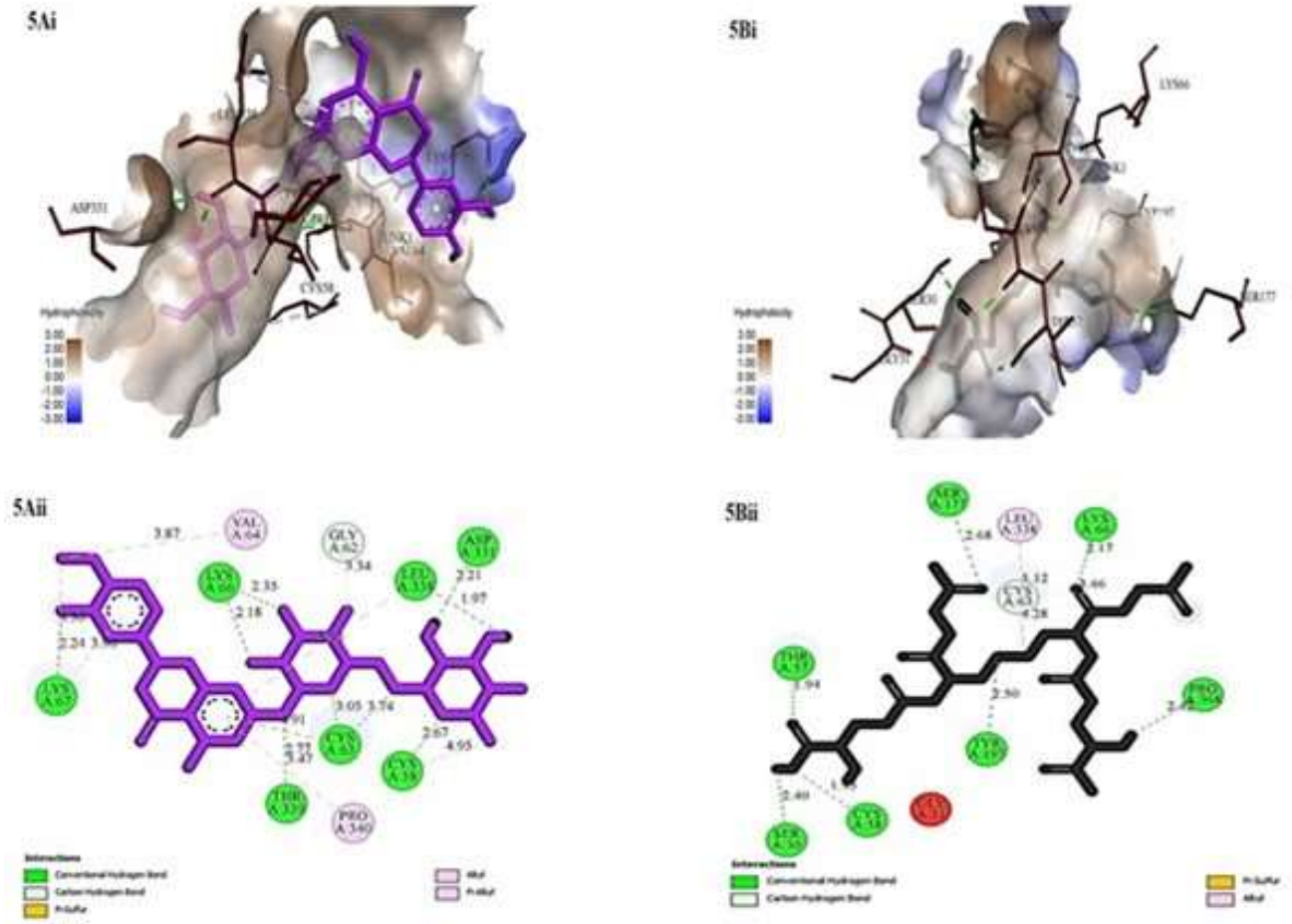

Figure 5. Molecular docking analysis of hesperidin and oxiglutathione with glutathione reductase. The figure illustrates the binding interactions of hesperidin and the standard inhibitor, oxiglutathione, within the active site of glutathione reductase. **(5A)** Hesperidin-glutathione reductase complex. **(5Ai)** Pocket hydrophobicity view, depicting the distribution of hydrophobic and hydrophilic regions within the binding site; **(5Aii)** Two-dimensional (2D) schematic representation of the specific amino acid residues involved in the interaction with hesperidin, including hydrogen bonds and other molecular contacts. **(5B)** Oxiglutathione-glutathione reductase complex. **(5Bi)** Pocket hydrophobicity view, showing the chemical environment of the binding site when occupied by the standard inhibitor, oxiglutathione; **(5Bii)** Two-dimensional (2D) schematic of the key amino acid residues and interactions between oxiglutathione and glutathione reductase.

The images collectively provide a detailed comparison of the binding modes and molecular interactions of hesperidin with the enzyme, relative to the known inhibitor, oxiglutathione.

3.1.4. Binding energy and docking sites of diosmin, hesperidin, diosmin-hesperidin conjugate, and PubChem-137348175 on Hsp 70. The binding affinities of the docked compounds were relatively higher than those of PubChem-137348175 (the standard inhibitor) (-6.5 Kcal/mol) on Hsp 70, with diosmin exhibiting the highest binding affinity (Figure 2D). Diosmin binds to Ala 412, Leu 413, Arg 416, Leu 413, Gln 424, Glu 446, and Arg 533 of Hsp 70 through the conventional hydrogen bond at the average bond distances of 3.46 Å, 2.40 Å, 2.51 Å, 2.40 Å, 2.21 Å, 1.99 Å, and 2.66 Å, respectively; Thr 425 through the relatively stronger carbon-hydrogen bond at the bond distance of 3.61 Å, as well as Lys 526 of the protein through the alkyl bond at the bond distance of 4.16 Å, following docking of the compounds into the protein (Figures 6Ai-6Aii). PubChem-137348175 (the standard inhibitor) binds to Ile 420, Ile 456, Leu 510 and Leu 486 of Hsp 70 through the hydrophobic alkyl bond at the average bond distance of 1.57 Å (Figures 6Bi -6Bii).

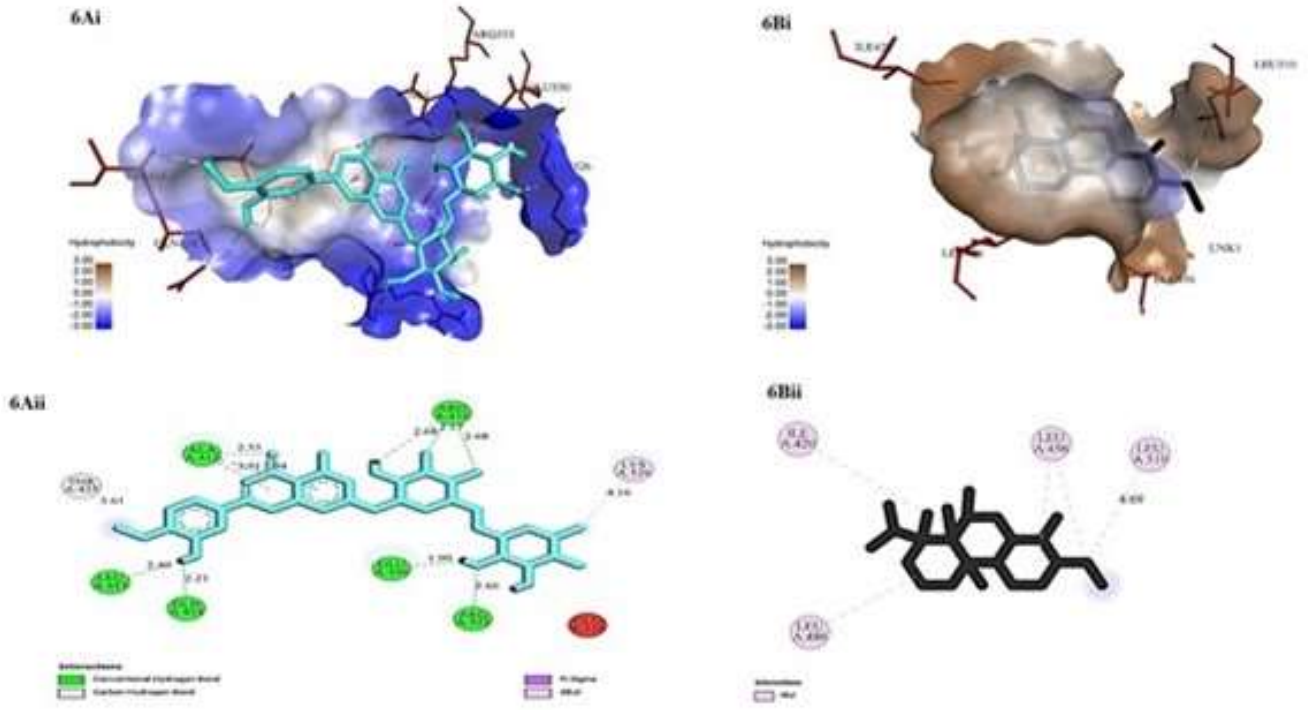

Figure 6. Binding interactions and pocket hydrophobicity of diosmin and a standard inhibitor with Hsp70. The figure illustrates the molecular interactions derived from docking simulations with the chaperone protein Hsp70.
(6A) Diosmin-Hsp70 Interactions: **(6Ai)** Depicts the hydrophobicity map of the Hsp70 binding pocket occupied by diosmin, revealing the nature of the microenvironment surrounding the ligand; **(6Aii)** shows the two-dimensional (2D) binding diagram of diosmin with Hsp70, detailing specific amino acid residues involved in hydrogen bonding and other key interactions.
(6B) PubChem-137348175-Hsp70 Interactions: **(6Bi)** displays the hydrophobicity map of the Hsp70 binding pocket with the standard inhibitor, PubChem-137348175; **(6Bii)** shows the two-dimensional (2D) binding diagram of the standard inhibitor, PubChem-137348175, with Hsp70, providing a reference for comparison with the diosmin interactions.

3.1.5. Binding energy and docking sites of diosmin, hesperidin, diosmin-hesperidin conjugate, and PubChem-137348175 on the Heat Shock Protein 90 Beta (Hsp 90ß). The binding affinities of the docked compounds were relatively higher than those of GLXC-04219 (the standard inhibitor) (-7.8 Kcal/mol) on heat shock protein 90ß (HSP 90ß) protein, with both diosmin and diosmin-hesperidin conjugate exhibiting the highest binding affinity of -10.3 Kcal/mol (Figure 2E). Thus, this makes these drugs ameliorate the DOX off-target toxicity and by inference the potential off-target organ toxicity

associated with use of Hsp 90 inhibitors such as geldanamycin. Diosmin binds to Asp 102 and Gly 97 of heat shock protein 90 beta (Hsp 90ß) through the conventional hydrogen bond at the bond distance of 3.47 Å and 2.68 Å; Trp 162, Phe 138, Tyr 139 through the relatively hydrophobic Pi-Pi stacked bond at the bond distances of 7.83 Å, 4.08 Å, 5.69 Å, as well as Leu 107 of the protein through the hydrophobic Pi-sigma bond at the distance of 4.53 Å, as well as Met 98 and Phe 170 at the distances of 5.42 Å and 4.71 Å following docking of the compounds into the protein (Figures 7Ai-7Aii). Similarly, diosmin-hesperidin conjugate binds to Trp 162, Gly 135, Asn 51, and Gly 71 on the Hsp 90ß through the conventional hydrogen bond at the bond distance of 3.76 Å, 1.92 Å, 2.62 Å, and 2.21 respectively; Phe 170, Met 98, Ile 96 through the relatively hydrophobic Pi-alkyl bond at the respective average bond distances of 4.76 Å, 4.97 Å, and 5.29 Å; Tyr 139 and Phe 138 of the protein through the hydrophobic Pi-Pi stacked bond at the respective distances of 5.70 Å and 4.09 Å, as well as Leu 107 through Pi-sigma bond at the distance of 1.74 Å following docking of the compounds into the protein (Figures 7Bi-17Bii). The standard Hsp 90ß inhibitor, GLXC-04219, also binds to Asp 93 of heat shock protein 90 beta (Hsp 90ß) through the conventional hydrogen bond at the average bond distance of 2.66 Å. This is in addition to Leu 107 and Leu 103 through the relatively stronger carbon-hydrogen bond at the respective average bond distances of 3.86 Å and 3.45 Å; Val 150, Ala 111, and Tyr 139 through the hydrophobic alkyl bond at the respective distances of 3.58 Å, 3.67 Å, and 3.02 Å, as well as Phe 138 and Asn 51 through the Amide-Pi stacked bond at the bond distances of 3.57 Å and 5.17 Å. GLXC-04219 also binds to Trp 162 and Met 98 of HSP 90ß protein through the hydrophobic Pi-sigma bond at the bond distances of 3.83 Å and 3.89 Å following docking of the compounds into the protein (Figure 7Ci-7Cii).

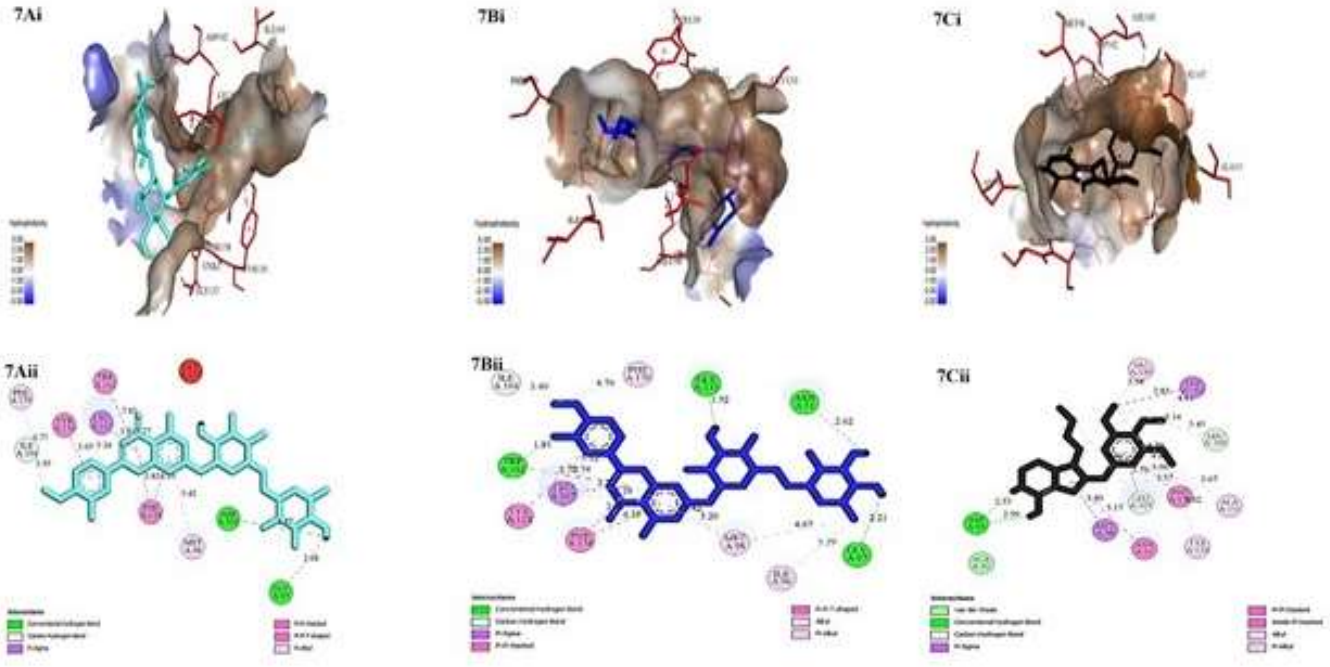

Figure 7. Molecular docking analysis of diosmin, the diosmin-hesperidin conjugate, and GLXC-04219 with Hsp90ß. The figure illustrates the binding interactions of diosmin, its conjugate, and the standard inhibitor GLXC-04219 within the binding pocket of the Hsp90ß protein.**(7A)** Interaction of diosmin with Hsp90ß. **(7Ai)** depicts the hydrophobicity of the binding pocket, while **(7Aii)** shows a 2D schematic of the specific amino acid residues involved in the interaction (e.g., hydrogen bonds and hydrophobic contacts).**(7B)** Interaction of the diosmin-hesperidin conjugate with Hsp90ß. **(7Bi)** shows the hydrophobicity of the binding pocket, and **(7Bii)** presents the 2D schematic of the ligand-protein interactions.**(7C)** Interaction of the standard inhibitor, GLXC-04219, with Hsp90ß. **(7Ci)** depicts the pocket hydrophobicity, and **(7Cii)** provides the 2D schematic of the binding interactions.

These visualizations provide a mechanistic insight into how each compound is predicted to bind to and potentially inhibit Hsp90ß, with more hydrophobic regions favoring interactions with nonpolar parts of the ligands.

3.1.6. Binding energy and docking sites of diosmin, hesperidin, diosmin-hesperidin conjugate, and BDBM50105195 on the Vascular Cell Adhesion Molecule 1 (VCAM-1) following docking simulation. The binding affinities of the docked compounds were relatively higher than those of BDBM50105195 (the standard inhibitor) (-5.7 Kcal/mol) on VCAM-1 protein, with hesperidin (-7.5 Kcal/mol) displaying the highest binding affinity (Figure 2F). Hesperidin binds to Phe 91, Tyr 89, Asp 17, Gln 14, and Leu 12 of VCAM-1 protein through the conventional hydrogen bond at the average bond distances of 2.51 Å, 2.20 Å, 2.19 Å, 4.23 Å, and 2.51 Å respectively; Arg 187 through the relatively hydrophobic Pi-cation bond at the bond distance of 5.12 Å; as well as Pro 184 and Val 19 through the Pi-alkyl bond at the bond distances of 5.00 Å and 4.23 Å, following docking of the compounds into the protein (Figures 8Ai-8Aii). Similarly, BDBM50105195 (the standard VCAM-1 protein inhibitor) binds to Lys 147, His 176, and Asp 122 of the VCAM-1 protein through the conventional hydrogen bond at the bond distances of 2.29 Å, 2.28 Å, and 2.19 Å, respectively; in addition to Arg 123 through the relatively hydrophobic Pi-alkyl bond at the bond distance of 4.65 Å, following docking of the compounds into the protein (Figure 8Bi-8Bii).

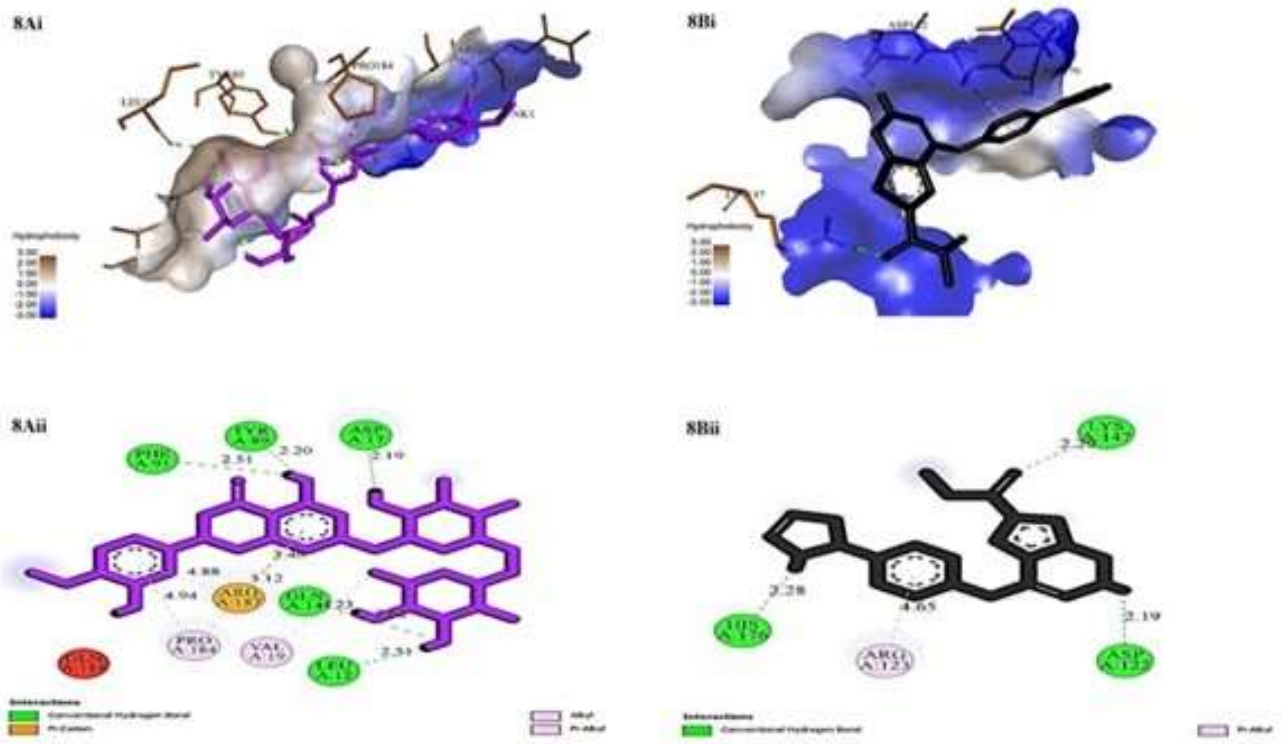

Figure 8. Molecular docking analysis of hesperidin and BDBM50105195 with VCAM-1. The figure illustrates the binding interactions of hesperidin and its standard inhibitor, BDBM50105195, with the active site of the VCAM-1 protein. **(8A)** Hesperidin-VCAM-1 interaction: **(8Ai)** Pocket hydrophobicity view: depicts the hydrophobic and hydrophilic characteristics of the VCAM-1 binding pocket, highlighting the environment where hesperidin binds; **(8Aii)** 2D interaction map: shows a two-dimensional schematic of the specific amino acid residues of VCAM-1 involved in hydrogen bonds and other molecular interactions with hesperidin. **(8B)** BDBM50105195-VCAM-1 interaction: **(8Bi)** Pocket hydrophobicity view: Illustrates the hydrophobic and hydrophilic properties of the VCAM-1 binding pocket in the context of BDBM50105195 binding; **(8Bii)** 2D interaction map: provides a two-dimensional diagram of the specific amino acid residues and types of bonds that BDBM50105195 forms with the VCAM-1 protein.

3.2. *In vitro* antioxidant studies of the graded concentrations of diosmin-hesperidin conjugate

These results show the antioxidant and scavenging activity of diosmin-hesperidin conjugate and the standard antioxidant drug (ascorbic acid) across *in vitro* assays such as DPPH, NO scavenging, FRAP, nitric oxide, lipid peroxidation inhibition, H_2O_2 scavenging, and total antioxidant capacity (TAC).

3.2.1. Effect of graded concentrations of diosmin-hesperidin conjugate on DPPH scavenging assay

The antioxidant activity of the diosmin-hesperidin conjugate was evaluated using the 2,2-diphenyl-1-picrylhydrazyl (DPPH) free radical scavenging assay. The conjugate demonstrated a concentration-dependent scavenging effect, with activity increasing from approximately 20% at 25µg/ml to 65% at 100µg/ml. This dose-response relationship yielded an estimated IC_{50} value of 79.85µg/ml. For comparative purposes, ascorbic acid, a well-established antioxidant standard, exhibited significantly higher radical scavenging potential across the tested concentrations, ranging from approximately 43% to 87%. The superior efficacy of ascorbic acid was quantitatively reflected in its lower IC_{50} value of 34.42µg/ml (Figure 9a).

3.2.2. Effect of graded concentrations of diosmin-hesperidin conjugate on NO scavenging assay

This assay measures the ability to neutralize nitric oxide, an important reactive species. Diosmin-hesperidin conjugate's scavenging activity ranges from ~23% at 25µg/ml to ~57% as the concentration increases to 100µg/ml with an IC_{50} value of 83.09 µg/ml. However, ascorbic acid shows a much stronger scavenging effect, with values from ~42% at 25µg/ml to ~74% at 100µg/ml and an estimated IC_{50} value of 38.86 µg/ml (Figure 9b).

3.2.3. Effect of graded concentrations of diosmin-hesperidin conjugate on ferric reducing antioxidant power (FRAP)

The ferric reducing antioxidant power (FRAP) assay, which measures the electron-donating capacity by quantifying the reduction of the ferric tripyridyltriazine complex (Fe^{3+}-TPTZ) to its ferrous form (Fe^{2+}-TPTZ), was also performed. The diosmin-hesperidin conjugate displayed a dose-dependent reducing activity, with FRAP values increasing from approximately 0.62 to 0.9. In contrast, ascorbic acid demonstrated a markedly higher reducing capacity, with FRAP values ranging from 1.04 to 1.63. These results corroborate the superior antioxidant potential of the ascorbic acid standard compared to the diosmin-hesperidin conjugate (Figure 9c).

3.2.4. Effect of graded concentrations of diosmin-hesperidin conjugate on lipid peroxidation inhibition

This assay measures the ability to prevent lipid peroxidation, which is important in preventing cell membrane damage. In this study, lipid peroxidation inhibition increased from ~28% at 25 µg/ml to ~62% at 100 µg/ml (Figure 9d) and with an estimated IC_{50} value of 80.55 µg/ml. However, ascorbic acid showed a stronger activity with inhibition ranging from ~40% at 25 µg/ml to ~76% at 100 µg/ml (Figure 9d) with an estimated IC_{50} value of 44.64 µg/ml.

3.2.5. Effect of graded concentrations of diosmin-hesperidin conjugate on H_2O_2 scavenging assay

Hydrogen peroxide (H_2O_2) scavenging assay measures the ability to neutralize hydrogen peroxide (H_2O_2). Diosmin-hesperidin's scavenging activity increased significantly from ~33% at 25µg/ml to ~73% at 100µg/ml, with an estimated IC_{50} value of 40.48 µg/ml. Again, in this assay, ascorbic acid exhibited a superior activity over diosmin-hesperidin conjugate in neutralizing H_2O_2 with its values ranging from ~74% at 25 µg/ml to ~90% at 100 µg/ml **(Figure 9e)**, and with an estimated IC_{50} value of 07.44 µg/ml

3.2.6. Effect of graded concentrations of diosmin-hesperidin conjugate on the total antioxidant capacity (TAC)

In this assay, diosmin-hesperidin conjugate exhibited an increased TAC values of 130.27 mg/100 g at 25 µg/ml to 132.24 mg/100 g at 100 µg/ml.

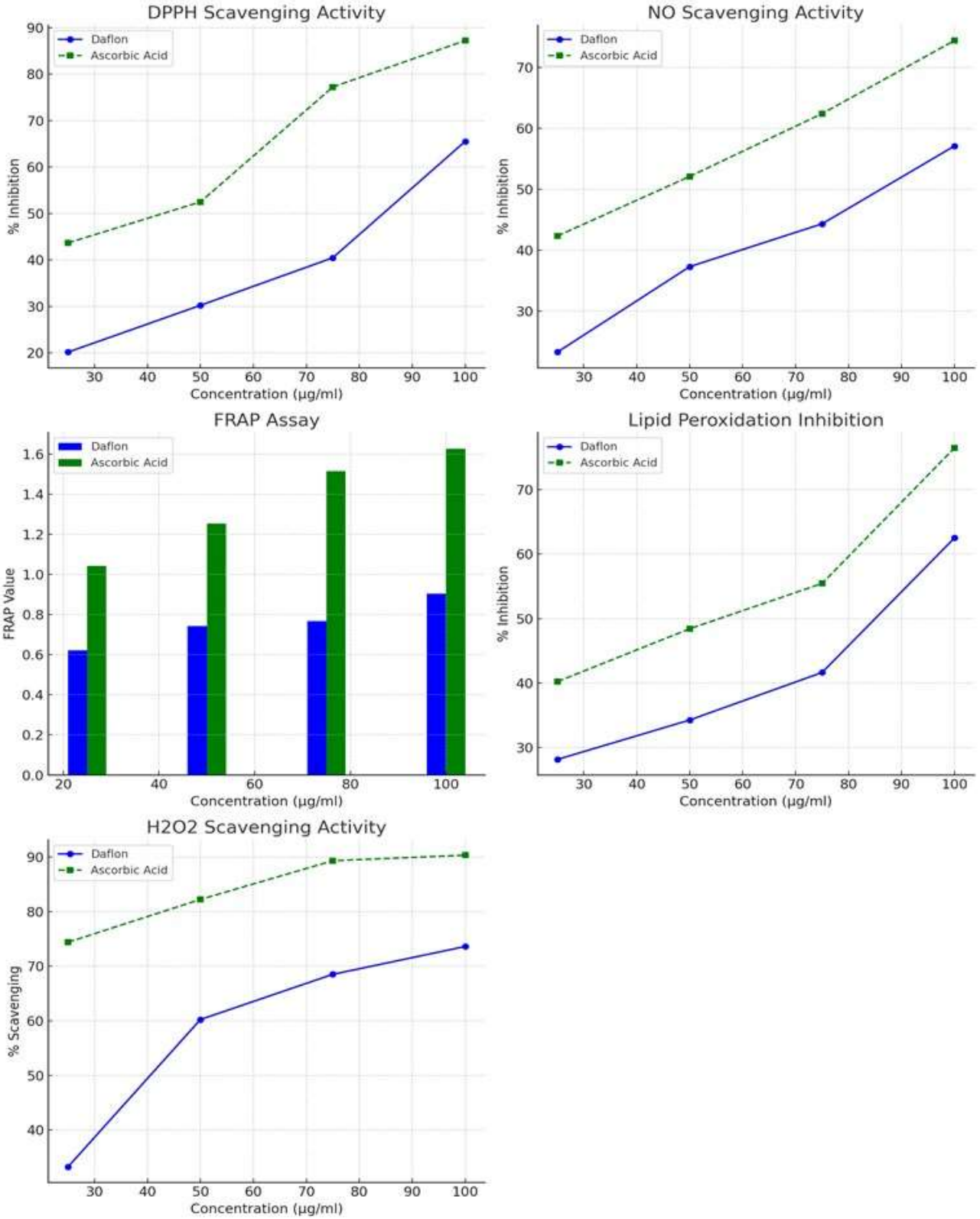

Figures 9a-9e. Activities of graded concentrations of diosmin-hesperidin conjugate of DPPH (Figure 9a), NO scavenging (Figure 9b), FRAP assay (Figure 9c), lipid peroxidation inhibition (Figure 9d) and hydrogen peroxide scavenging (Figure 9e) capabilities.

4. Discussion

This study evaluated the therapeutic potential of a diosmin-hesperidin conjugate in mitigating doxorubicin (DOX)-induced organ toxicities, with a focus on cardiac, hepatic, and renal systems. Utilizing integrated *in silico* molecular docking and *in vitro* antioxidant assays, the underlying protective mechanisms were systematically elucidated. Despite significant advances in cancer chemotherapy and drug delivery systems that have improved survival and quality of life for cancer patients [25], off-target toxicities, especially cardiotoxicity, remain a major limitation. This adverse effect often manifests as reduced left ventricular ejection fraction (LVEF) and may necessitate therapy discontinuation, increasing the risk of disease relapse and poor clinical outcomes [26-28]. DOX, a widely used anthracycline chemotherapeutic, inflicts multi-organ damage through mechanisms involving oxidative stress, topoisomerase II inhibition, and apoptosis induction [29,30]. Its cytotoxicity arises from DNA intercalation, disruption of topoisomerase II function, reactive oxygen species (ROS) generation, and activation of diverse cell death pathways including apoptosis, autophagy, and ferroptosis [2,3,31]. Organ toxicity has been specifically linked to inhibition of topoisomerase IIß, highly expressed in healthy tissues [14,32,33], making modulation of these pathways a promising strategy to reduce DOX-induced injury [34]. Molecular docking revealed strong binding affinities between the diosmin-hesperidin conjugate and key proteins involved in apoptosis and oxidative stress, including caspase-3, catalase, Hsp70, Hsp90ß, and VCAM-1. Heat shock proteins (Hsps), such as Hsp70 and Hsp90, function as molecular chaperones and are upregulated under cellular stress [35-37]. Hsp70 is a established biomarker of DOX toxicity, associated with myocardial inflammation, fibrosis, and adverse remodeling [38]. It modulates apoptosis by inhibiting cytochrome c release and caspase activation [39], making it a relevant target for cardioprotection. The high binding affinity of the conjugate to Hsp70 suggests potential anti-apoptotic effects.

Conversely, Hsp90 supports oncogenic client proteins and is a target in anticancer therapy [40]. While the conjugate demonstrated high affinity for Hsp90, selectivity between cancerous and healthy isoforms remains a concern [35]. While healthy cells predominantly express a constitutive form of Hsp90, cancer cells overexpress the stress-inducible variant [35]. An ideal inhibitor would selectively target the cancer-specific form. However, further *in vitro* and *in vivo* studies are needed to assess whether the conjugate can selectively inhibit cancer-specific Hsp90 without affecting constitutive forms in normal tissues. The diosmin-hesperidin conjugate and its precursors exhibited consistently stronger binding affinities (more negative values) across all six protein targets compared to reference compounds, indicating multi-target engagement against apoptosis, oxidative stress, and inflammation. Interaction analyses revealed complex binding modes involving hydrogen bonding, hydrophobic contacts, and ionic interactions, supporting stable target engagement. For instance, caspase-3 inhibition involved key residues such as Thr140 and Phe158 through mixed bonding types, suggesting potent and specific activity. *In vitro* assays further confirmed the conjugate's potent concentration-dependent antioxidant activity across multiple models, consistent with previous reports on diosmin and hesperidin [41-47]. Although ascorbic acid showed superior reducing power and lipid peroxidation inhibition in certain assays, the conjugate demonstrated significant radical scavenging and total antioxidant capacity, supporting its role in mitigating oxidative damage. Notably, while dexrazoxane, an FDA-approved cardioprotectant, was originally thought to act via iron chelation and antioxidant mechanisms, recent evidence points to topoisomerase IIß inhibition as its primary mode of action [49,50]. Its limited efficacy in vascular oxidative contexts [51] contrasts with the broad antioxidant profile of N-acetylcysteine (NAC), which enhances glutathione synthesis and directly neutralizes ROS [52–54]. The diosmin-hesperidin conjugate, with its multi-mechanistic antioxidant and anti-apoptotic properties, may offer a complementary or superior alternative in non-cardiotoxicity-related ROS conditions.

5. Conclusions

The integrated computational and experimental *in vitro* findings highlight the inherent potential of the diosmin-hesperidin conjugate as a multi-mechanistic agent against DOX-induced toxicities. The protective effects are likely mediated through a combination of anti-apoptotic, antioxidant, and endothelial protective mechanisms, highlighting the therapeutic potential of this fixed-dose combination in cancer chemotherapy. However, its polypharmacological profile warrants further investigation to confirm selective cytotoxicity and

safety in preclinical models, particularly regarding Hsp90 isoform specificity and organ-specific protection.

Acknowledgement: The authors sincerely appreciate the technical support provided by Dr. Temidayo O. Adigun of the Department of Biochemistry, University of Ilorin, Ilorin, Kwara State, Nigeria and Mr. Sunday O. Adenekan (Chief Technologist) of the Department of Medical Biochemistry, College of Medicine, University of Lagos, Idi-Araba, Lagos State, Nigeria, in the areas of molecular docking studies and *in vitro* antioxidant analysis, respectively.

Conflicts of Interest: The authors declare no conflict of interest

Funding: The authors received no financial support for the research, authorship, and/or publication of this article.

Abbreviations

ANOVA	analysis of variance
BAX	BCL-2-associated X Protein
BCL-2	B cell lymphoma/leukemia type 2
DNA	deoxyribonucleic acid
DOX	doxorubicin
DPPH	1, 1- diphenyl-2-picryl hydrazyl
FRAP	ferric reducing antioxidant power
GSH	reduced glutathione
H_2O_2	hydrogen peroxide
Hsp 70	heat shock protein 70
Hsp 90ß	heat shock protein 90 beta
IC_{50}	inhibitory concentration 50
1GRE	glutathione reductase binding substrate
LVEF	left ventricular ejection fraction
MSN-125	Bax/Bak oligomerization inhibitor
NAC	N-acetylcysteine
NO	nitric oxide
ROS	reactive oxygen species
S.E.M.	standard error of the mean
SNP	sodium nitroprusside
TAC	total antioxidant capacity
VCAM 1	Vascular Cell Adhesion Molecule 1

References

[1] Carvalho, C.; Santos, R. X.; Cardoso, S.; Correia, S.; Oliveira, P. J.; Santos, M.S.; Moreira, P.I. "Doxorubicin: The good, the bad and the ugly effect". Curr. Med. Chem., 16(25): 3267-3285, 2009. https://doi.org/10.2174/092986709788803312.

[2] Kciuk, M.; Gielecińska, A.; Mujwar, S.; Kołat, D.; Kałuzińska-Kołat, Ż.; Celik, I.; Kontek, R. "Doxorubicin - An agent with multiple mechanisms of anticancer activity". Cells, 12(4): 659, 2023. https://doi.org/10.3390/cells12040659.

[3] Adeneye, A.A.; Babatope, F.E.; Adesiji-Adelekan, A.E.; Olorundare, O.E.; Okoye, I.I. "Tadalafil pretreatment attenuates doxorubicin-induced hepatorenal toxicity by modulating oxidative stress and inflammation in Wistar rats". Toxicol. Rep., 13: 101737, 2024. https://doi.org/10.1016/j.toxrep.2024.101737.

[4] Boeno, F.P.; Patel, J.; Montalvo, R.N.; Lapierre-Nguyen, S.S.; Schreiber, C.M.; Smuder, A.J. "Effects of exercise preconditioning on doxorubicin-induced liver and kidney toxicity in male and female rats". Intl. J. Mol. Sci., 24(12): 10222, 2023. https://doi.org/10.3390/ijms241210222.

[5] Renu, K.; Pureti, L.P.; Vellingiri, B.; Valsala Gopalakrishnan, A. "Toxic effects and molecular mechanism of doxorubicin on different organs – an update". Toxin Reviews, 41(2): 650-674, 2021. https://doi.org/10.1080/15569543.2021.1912099

[6] Kumar, S.; Pandey, A.K. "Chemistry and biological activities of flavonoids: An overview". Sci. World J., 2013: 162750, 2013. https://doi.org/10.1155/2013/162750

[7] Osama, H.; Hamed, E.O.; Mahmoud, M.A.; Abdelrahim, M.E.A. "The effect of hesperidin and diosmin individually or in combination on metabolic profile and neuropathy among diabetic patients with metabolic syndrome: A randomized controlled trial". J. Diet Suppl., 20(5): 749-762, 2023. https://doi.org/10.1080/19390211.2022.2107138.

[8] Wójciak, M.; Feldo, M.; Borowski, G.; Kubrak, T.; Płachno, B.J.; Sowa, I. "Antioxidant potential of diosmin and diosmetin against oxidative stress in endothelial cells." Molecules, 27(23): 8232, 2022. https://doi.org/10.3390/molecules27238232

[9] Yasım, A.; Özbağ, D.; Kılınç, M.; Çıralık, H.; Toru, İ. "The effect of diosmin-hesperidin combination treatment on the lipid profile and oxidative-antioxidative system in high-cholesterol diet-fed rats." Turkish J. Thorac. Cardiovasc. Surg., 19(1): 55-61, 2011.

https://tgkdc.dergisi.org/uploads/pdf/pdf_TGKDC_1353.pdf
[10] Ahmed, O.M.; Elkomy, M.H.; Ashour, M.B.; Mahmoud, H.U.R.; Naguib, I.A.; Fahim, H.I.; Alghamdi, B.S.; Ahmed, N.A. "Rutin and quercetin counter doxorubicin-induced liver toxicity in Wistar rats via their modulatory effects on inflammation, oxidative stress, apoptosis, and Nrf2." Oxid. Med. Cell. Longev., 2022: 2710607, 2022. https://doi.org/10.1155/2022/2710607
[11] Chandimali, N.; Bak, S.G.; Park, E.H.; Lim, H-J.; Won, Y-S.; Kim, E-K., Park, S-I.; Lee, S.J. "Free radicals and their impact on health and antioxidant defenses: a review." Cell Death Discov., 11: 19, 2025. https://doi.org/10.1038/s41420-024-02278-8
[12] Morgan, E.M.; Boltia, S.A.; Fayez, Y.M.; Abdelkawy M; Lotfy HM. "Coupling of physical extraction and mathematical filtration in spectrophotometric analysis of natural therapy essential for prophylaxis and treatment of COVID-19 infection - Comparative study along with greenness evaluation". Heliyon, 9(6): e16284, 2023. https://doi.org/10.1016/j.heliyon.2023.e16284
[13] Fatoki, T.H.; Balogun, T.C.; Ojewuyi, A.E.; Omole, A.C.; Olukayode, O.V.; Adewumi, A.P.; Umesi, A.J.; Ijeoma, N.P.; Apooyin, A.E.; Chinedu, C.P.; Idowu, I.E.; Isah, M.J. "*In silico* molecular targets, docking, dynamics simulation and physiologically based pharmacokinetics modeling of oritavancin". BMC Pharmacol. Toxicol., 25: 79, 2024. https://doi.org/10.1186/s40360-024-00804-z
[14] Dhuli, K.; Bonetti, G.; Anpilogov, K.; Herbst, K.L.; Connelly, S.T.; Bellinato, F.; Gisondi, P.; Bertelli, M. (2022). "Validating methods for testing natural molecules on molecular pathways of interest *in silico* and *in vitro*. J. Prev. Med. Hyg., 63(2 Suppl. 3): E279-E288, 2022. https://doi.org/10.15167/2421-4248/jpmh2022.63.2S3.2770
[15] Patil, N.; Mirveis, Z.; Byrne, H.J. (2024), "Kinetic modelling of the cellular metabolic responses underpinning *in vitro* glycolysis assays". FEBS Open Bio, 14: 466-486, 2024. https://doi.org/10.1002/2211-5463.13765
[16] Trott, O.; Olson, A.J. "AutoDock Vina: Improving the speed and accuracy of docking with a new scoring function, efficient optimization and multi-threading. J. Comput. Chem., 31: 455-461, 2010. https://doi.org/10.1002/jcc.21334
[17] López-López, E.; Naveja, J.J.; Medina-Franco, J.L. (2019). "DataWarrior: An evaluation of the open-source drug discovery tool" Expert Opin. Drug Discov., 15: 13-17, 2019. https://doi.org/10.1080/17460441.2019.1581170
[18] Du, X.; Li, Y.; Xia, Y.L.; Ai, S.M.; Liang, J.; Sang, P. "Insights into protein-ligand interactions: mechanisms, models, and methods". Int. J. Mol. Sci., 17: 144-147, 2016. https://doi.org/10.3390/ijms17020144
[19] Baroroh, U.; Si. S.; Biotek, M.; Muscifa, Z.S.; Destiarani, W.; Rohmatullah, F.G.; Yusuf. M. "Molecular interaction analysis and visualization of protein-ligand docking using Biovia Discovery Studio Visualizer". Indonesian J. Comput. Biol., 2(1): 22-30, 2023.
[20] Hussen, E.M.; Endalew, S.A. "*In vitro* antioxidant and free-radical scavenging activities of polar leaf extracts of *Vernonia amygdalina*". BMC Complement. Med. Ther., 23, 146 (2023). https://doi.org/10.1186/s12906-023-03923-y
[21] Etim, O.E.; Ekanem S.E.1.; Sam, S.M. "*In vitro* antioxidant activity and nitric oxide scavenging activity of *Citrullus lanatus* seeds". J. Nat. Sci. Res., 3(12): 126-132, 2013. https://core.ac.uk/download/pdf/234654281.pdf
[22] Gülçin, İ.; Huyut, Z.; Elmastaş, M.; Aboul-Enein, H.Y. "Radical scavenging and antioxidant activity of tannic acid". Arab. J. Chem. 3(1): 43-53, 2010. https://doi.org/10.1016/j.arabjc.2009.12.008
[23] Vishwakarma, A.; Wany, A.; Pandey, S.; Bulle, M.; Kumari, A.; Kishorekumar, R.; Igamberdiev, A.U.; Mur, L.A.J.; Gupta, K.J. "Current approaches to measure nitric oxide in plants". J. Exp. Bot., 70(17) (2019), 4333-4343. https://doi.org/10.1093/jxb/erz242
[24] Peach, M.L.; Beedie, S.L.; Chau, C.H.; Collins, M.K.; Markolovic, S.; Luo, W.; Tweedie, D.; Steinebach, C.; Greig, N.H.; Gütschow, M.; Vargesson, N.; Nicklaus, M.C.; Gigg, W.D. (2020). "Antiangiogenic activity and in silico cereblon binding analysis of novel thalidomite analogs". Molecules, 25(23): 5683. https://doi.org/10.3390/molecules25235683
[25] Hoeh, B.; Würnschimmel, C.; Flammia, R.S.; Horlemann, B.; Sorce, G.; Chierigo, F.; Tian, Z.; Saad, F.; Graefen, M.; Gallucci, M.; Briganti, A.; Terrone, C.; Shariat, S.F.; Tilki, D.; Kluth, L.A.; Mandel, P.; Chun, F.K.H.; Karakiewicz, P.I. "Effect of chemotherapy on overall survival

in contemporary metastatic prostate cancer patients". Front. Oncol. 11:778858. https://doi.org/10.3389/fonc.2021.778858

[26] Copeland-Halperin, R.S.; Al-Sadawi, M.; Patil, S.; Liu, J.E.; Steingart, R.M.; Dang, C.T.; Yu, A.F. "Early trastuzumab interruption and recurrence-free survival in ERBB2-positive breast cancer". JAMA Oncol., 6(12):1971-1972, 2020. https://doi.org/10.1001/jamaoncol.2020.4749.

[27] Mudd, T.W. Jr.; Khalid, M.; Guddati, A.K. "Cardiotoxicity of chemotherapy and targeted agents". Am. J. Cancer Res., 11(4):1132-1147, 2021. https://pmc.ncbi.nlm.nih.gov/articles/PMC8085845/

[28] Mattioli, R.; Ilari, A.; Colotti, B.; Mosca, L.; Fazi, F.; Colotti, G. "Doxorubicin and other anthracyclines in cancers: Activity, chemoresistance and its overcoming". Mol. Asp. Med., 93: 101205, 2023. https://doi.org/10.1016/j.mam.2023.101205

[29] Patil, P.P.; Kumar, P., Khanal, P.; Patil, V.S.; Darasaguppe, H.R.; Bhandare, V.V.; Bhatkande, A.; Shukla, S.; Joshi, R.K.; Patil, B.M.; Roy, S. "Computational and experimental pharmacology to decode the efficacy of *Theobroma cacao* L. against doxorubicin-induced organ toxicity in EAC-mediated solid tumor induced mice". Front. Pharmacol. 2023; 14:1174867, 2023. https://doi.org/10.3389/fphar.2023.1174867

[30] Thorn, C.F.; Oshiro, C.; Marsh, S.; Hernandez-Boussard, T.; McLeod, H.; Klein, T.E.; Altman, R.B. "Doxorubicin pathways: pharmacodynamics and adverse effects". Pharmacogenet Genom, 21(7): 440-446, 2011. https://doi.org/10.1097/FPC.0b013e32833ffb56

[31] Adeneye, A.A.; Olorundare, O.E.; Akinsola, A.O.; Sanni, D.A.; Okoye, I.I.; Ntambi, J.M.; Mukhtar, H. "Ameliorative potential of *Clerodendrum volubile* ethanol leaf extract on doxorubicin-induced hepatorenal toxicities in rats". Pharmacol. Toxicol. Nat. Med., 1(1): 1-13, 2021. https://doi.org/10.52406/ptnm.v1i1.8

[32] Nitiss, J.L. "Targeting DNA topoisomerase II in cancer chemotherapy'. Nat Rev Cancer, 9(5): 338-50, 2009. https://doi.org/10.1038/nrc2607

[33] Baikar, S.; Malpathak, N. "Secondary metabolites as DNA topoisomerase inhibitors: A new era towards designing of anticancer drugs". Phcog. Rev., 4(7): 12-26, 2010. https://doi.org/10.4103/0973-7847.65320

[34] Yan, T.; Yu, H.; Li, T.; Dong, Y. "Mechanisms of cardiovascular toxicities induced by cancer therapies and promising biomarkers for their prediction: A scoping review". Heart Lung Circ., 33: 605-638, 2024. https://doi.org/10.1016/j.hlc.2023.12.006

[35] Birbo, B.; Madu, E.E.; Madu, C.O.; Jain, A.; Lu, Y. "Role of HSP90 in Cancer." Int. J. Mol. Sci., 22: 10317, 2021. https://doi.org/10.3390/ijms221910317

[36] Wei, H.; Zhang, Y.; Jia, Y.; Chen, X.; Niu, T.; Chatterjee, A.; He, P.; Hou, G. "Heat shock protein 90: biological functions, diseases, and therapeutic targets". MedComm., 5: e470, 2024. https://doi.org/10.1002/mco2.47

[37] Singh, M.K., Shin, Y., Ju, S., Han, S., Choe, W., Yoon, K.S., Kim, S.S., Kang, I. "Heat shock response and heat shock proteins: current understanding and future opportunities in human diseases". Int. J. Mol. Sci., 25(8): 4209, 2024. https://doi.org/10.3390/ijms25084209

[38] Liu, P., Bao, H-Y., Jin, C-C., Zhou, J-C., Hua, F., Li, K., Lv, X-X., Cui, B., Zhuo-Wei Hu, Z-W., Zhang, X-W. "Targeting extracellular heat shock protein 70 ameliorates doxorubicin-induced heart failure through resolution of toll-like receptor 2-mediated myocardial inflammation". JAHA, 8: e012338, 2019. https://doi.org/10.1161/JAHA.119.012338.

[39] Demidenko, Z.; Vivo, C.; Halicka, H.D.; Li, C.J.; Bhalla, K.; Broude, E.V.; Blagosklonny, M.V. "Pharmacological induction of Hsp70 protects apoptosis-prone cells from doxorubicin: comparison with caspase-inhibitor- and cycle-arrest-mediated cytoprotection". Cell Death Differ., 13: 1434-1441, 2006. https://doi.org/10.1038/sj.cdd.4401812

[40] Whitesell, L.; Lindquist, S.L. "Hsp 90 and the chaperoning of cancer". Nat. Rev. Cancer, 5(10): 761-772, 2005. https://doi.org/10.1038/nrc1716

[41] Hajimahmoodi, M.; Moghaddam, G.; Mousavi, S.M.; Sadeghi, N.; Oveisi. M.R.; Jannat, B. "Total antioxidant activity, and hesperidin, diosmin, eriocitrin and quercetin contents of various lemon juices". TJPR, 13(6): 951-956, 2014. https://doi.org/10.4314/tjpr.v13i6.18

[42] Lee, H.J.; Lee, S.H.; Hong, S.K.; Gil, B.I.; Lee KA. "*In vitro* biological activities of hesperidin-related compounds with different solubility. Antioxidants (Basel), 13(6): 727. https://doi.org/10.3390/antiox13060727.

[43] Choi, S.S.; Lee, S.H.; Lee, K.A. "A comparative study of hesperetin, hesperidin, and hesperidin glucoside: antioxidant, anti-Inflammatory, and

antibacterial activities *in vitro*. Antioxidants (Basel), 11(8): 1618, 2022. https://doi.org/10.3390/antiox11081618.

[44] Rajasekar, M; Baskaran, P.; Mary, J.; Sivakumar, M.; Selvam, M. "Revisiting diosmin for their potential biological properties and applications". Carbohydr. Polym. Technol. Appl., 7: 100419, 2024. https://doi.org/10.1016/j.carpta.2023.100419.

[45] Yasım, A.; Özbağ, D.; Kılınç, M.; Çıralık, H.; Toru, I. "The effect of diosmin-hesperidin combination treatment on the lipid profile and oxidative-antioxidative system in high-cholesterol diet-fed rats". Turk. J. Thorac. Cardiovasc. Surg., 19(1): 55-561, 2011.

[46] Huwait, E.; Mobashir, M. "Potential and therapeutic roles of diosmin in human diseases". Biomedicines, 10(5): 1076, 2022. https://doi.org/10.3390/biomedicines10051076

[47] Shaaban, H.H.; Hozayen, W.G.; Khaliefa, A.K.; El-Kenawy, A.E.; Ali, T.M.; Ahmed, O.M. (2022). "Diosmin and trolox have anti-arthritic, anti-inflammatory and antioxidant potencies in complete Freund's adjuvant-induced arthritic male Wistar rats: roles of NF-κB, iNOS, Nrf2 and MMPs". Antioxidants, 11(9): 1721, 2022. https://doi.org/10.3390/antiox11091721

[48] Lebrecht, D.; Geist, A.; Ketelsen, U.P.; Haberstroh, J.; Setzer, B.; Walker, U.A. "Dexrazoxane prevents doxorubicin-induced long-term cardiotoxicity and protects myocardial mitochondria from genetic and functional lesions in rats." Br. J. Pharmacol., 151(6): 771-778, 2007. https://doi.org/10.1038/sj.bjp.0707294

[49] Che, F.; Liu, Y.; Xu, C. "Prevention and treatment of doxorubicin-induced cardiotoxicity by dexrazoxane and Schisandrin B in rabbits." Int. J. Toxicol., 30(6): 681-689, 2011. https://doi.org/10.1177/1091581811415873

[50] Jirkovsky, E.; Jirkovská, A.; Bavlovič-Piskáčková, H.; Skalická, V.; Pokorná, Z.; Karabanovich, G.; Kollárová-Brázdová, P.; Kubeš, J.; Lenčová-Popelová, O.; Mazurová, Y.; Adamcová, M.; Lyon, A.R.; Roh, J.; Šimůnek, T.; Štěrbová-Kovaříková, P.; Štěrba, M. "Clinically translatable prevention of anthracycline cardiotoxicity by dexrazoxane is mediated by topoisomerase II beta and not metal chelation." Circ Heart Fail, 14(11): e008209, 2021. https://doi.org/10.1161/CIRCHEARTFAILURE.120.008209

[51] Bosman, M.; Krüger, D.N.; Favere, K.; De Meyer, G.R.Y.; Franssen, C.; Van Craenenbroeck, E.M.; Guns, P-J. "Dexrazoxane does not mitigate early vascular toxicity induced by doxorubicin in mice." PLoS ONE, 18(11): e0294848, 2023. https://doi.org/10.1371/journal.pone.0294848

[52] Arica, V.; Demir, İ.H.; Tutanc, M.; Basarslan, F.; Arica, S.; Karcoıglu, M.; Öztürk, H.; Nacar, A. "N-acetylcysteine prevents doxorubucin-induced cardiotoxicity in rats." Hum Exp Toxicol., 32(6): 655–61, 2013. https://doi.org/10.1177/0960327112467043

[53] Khazdooz, H.; Nourian, M.; Jalaeikhoo, H.; Rajaeinejad, M.; Moghadam, A.J.; Iranpour, M.; Naghoosi, H.; Tofangchiha, S. "The effect of N-acetylcysteine administration to prevent anthracycline-induced cardiotoxicity in breast cancer patients. Multidiscip. Cancer Investig., 3(3): 16-19, 2019. https://doi.org/10.30699/acadpub.mci.3.3.16

[54] Mahmoud, E.; Hussien, R.; George, S.;Refaiy, A.; Radwan, R.A. "The role of N-acetyl cysteine in ameliorating doxorubicin induced cardiotoxicity in rats." Zagazig J. Forensic Med. Toxicol., 20(2): 319-338, 2022. https://doi.org/10.21608/zjfm.2021.71789.1075.